processes

MDPI

Article

On the Location and Accessibility of Active Acid Sites in MFI Zeolites Modified by Alkaline Treatment

Lucas G. Tonutti , Lourdes Vergara , Carlos A. Querini and Bruno O. Dalla Costa *

Instituto de Investigaciones en Catálisis y Petroquímica "Ing. José Miguel Parera" (INCAPE), CONICET/UNL, Colectora RN 168 s/n, Santa Fe ZC 3000, Argentina; ltonutti@fiq.unl.edu.ar (L.G.T.); lvergara@fiq.unl.edu.ar (L.V.); querini@fiq.unl.edu.ar (C.A.Q.)

* Correspondence: bdallacosta@fiq.unl.edu.ar; Tel.: +54-342-4511370 (ext. 6033)

Abstract: An MFI zeolite (Si/Al = 40) was desilicated by alkaline treatment in order to generate mesopores. Temperature, alkali concentration and treatment duration were adjusted to maximize mesoporosity while preserving the zeolite structure. Special attention was paid to the characterization of the strength and accessibility of the acid sites. The catalysts were tested in the isobutane/butene alkylation, a reaction that is typically catalyzed by zeolites but limited by coke deposition. Additionally, glycerol esterification with acetic acid was used as a test reaction due to the required participation of large pores. The results confirmed that mesopores were successfully generated in the MFI zeolite, and the diffusion through the solid was enhanced, but the active sites were mainly confined to the micropores.

Keywords: MFI; alkylation; esterification; mesopores; acidity

check for updates

Citation: Tonutti, L.G.; Vergara, L.; Querini, C.A.; Dalla Costa, B.O. On the Location and Accessibility of Active Acid Sites in MFI Zeolites Modified by Alkaline Treatment. *Processes* **2024**, *12*, 2567. https://doi.org/10.3390/pr12112567

Academic Editor: Maria Victoria López Ramón

Received: 15 October 2024
Revised: 9 November 2024
Accepted: 13 November 2024
Published: 16 November 2024

1. Introduction

Zeolites have been successfully employed as catalysts in numerous reactions due to their stable and well-ordered structure, high surface area and tunable acidity. However, their microporous structure imposes diffusive restrictions and makes them susceptible to deactivation by fouling and coke deposition. To overcome these limitations, several techniques have been developed to synthesize hierarchical zeolites, which combine microporous and mesoporous pore networks [1–3]. These methods include syntheses in the presence of a template [4–6], alkaline treatments [4,7–10], acid leaching [10], steaming [4], layering [11] and pillaring [11,12].

Top–down methods are those that involve the partial dissolution of the lattice to generate mesoporosity and improve the overall mass transfer through the structure [10,13]. Steaming and acid leaching conduce to the dealumination of the framework. These procedures are suitable for low Si/Al materials, and, since they involve selective aluminum removal, they reduce the amount of acid sites, as well as the crystallinity, while the generated cavities might lack connectivity [12,14]. On the contrary, alkaline treatment selectively removes silicon atoms from the framework and its speed and extent increase in zeolites with low aluminum content. This behavior is attributed to the difference in solubility of silica and alumina at pH values above 9.5 [15,16], to the point where Al atoms prevent the dissolution of neighboring Si atoms [17]. Framework defects are also attacked preferentially [18]. Therefore, the main variables to be considered are the Si/Al ratio of the parent material, the temperature, duration, the alkali used and its concentration. Early studies by Ogura et al. [19] set the conditions for treating MFI zeolites while avoiding significant loss of material. Later, Groen et al. [20–22] explored a wide range of variables and their influence on structural properties, finding that the alkaline treatment did not affect the acidity of the materials. Tzoulaki et al. [4] also found that the alkaline treatment had no influence on the Brønsted acid sites in the micropores but reported an increase in site accessibility. Further steaming of the treated zeolite led to a decrement in acid sites concentration.

Overall, different variables affect mesoporosity development in different ways:

- Si/Al ratio: Since Al atoms protect neighboring Si atoms, high-aluminum zeolites are rarely attacked by alkali solutions. On the other hand, low-aluminum zeolites suffer from extensive removal of silicon, with significant destruction of the framework. Thus, the optimum range for the application of this method is Si/Al = 15–50 [21,23–26].
- Temperature: Temperature's effect is dual. On the one hand, an increase in temperature leads to an increase in solubility for both silicates and aluminates, decreasing the selectivity of the treatment. On the other hand, the process is very slow at temperatures below 25 °C, with the optimum temperature being between 30 and 70 °C [21,27].
- Time: The process follows an exponential trend, where most silicon removal occurs in the first 30 min of treatment. After 60 min, the rate becomes rather slow [21,27,28].
- Alkali: The treatment requires strong bases. It was found that kinetics follow the order LiOH < NaOH < KOH, in accordance with the effective ionic diameter of the cations. However, NaOH is more conducive to mesoporosity development than KOH, since silicate anions are more stable in the presence of Na^+, preventing silica redeposition [21]. Weak bases (for example, $NaHCO_3$ or tetraalkylammonium hydroxides) lead to very slow silicon removal, and have proven useful for generating mesopores in a controlled way over low-aluminum frameworks [25,29,30].
- Alkali concentration: The alkali concentration reflects the aggressiveness of the treatment. Higher concentrations lead to higher silicon removal and porosity generation, as well as lower yields and, ultimately, framework collapse [27]. The optimum concentration depends strongly on the Si/Al ratio of the parent material and its crystalline structure [23–25,31].
- Zeolite compensation cation: Identical results have been obtained for zeolites in protonic, ammonic or sodic forms, rendering this factor irrelevant to the treatment [21,30].
- Zeolite structure: As mentioned, defects are preferentially attacked; therefore, zeolites with partially amorphous frameworks are more susceptible to treatment [32,33]. Moreover, cage-like zeolites are more prone to collapse due to T-atom removal than channel-like zeolites [27].

In recent decades, the exploitation of nonconventional sources of oil and gas has increased significatively. The US, Canada, Argentina and China produced a combined yearly total of about 9×10^{11} m^3 shale gas, which is expected to increase in the coming decades [34]. Like natural gas, it consists mainly of methane, but might include significant amounts of ethane, propane, butane and pentane (in some cases, up to 15%), as well as CO_2 and N_2 [35–37]. In this context, C-C coupling reactions gain relevance for obtaining valuable compounds from these short alkanes and alkenes [38].

The alkylation of isobutane with butenes is a reaction of addition, which yields trimethylpentanes (TMPs) as products of interest (Scheme 1). This mixture of multi-branched isoparaffins (also known as alkylated product) presents high octane numbers (RON and MON), low vapor pressure and null sulfur content, making it an interesting contributor to gasoline blending. The reaction is catalyzed by strong acids, and current industrial units typically operate either with HF or with H_2SO_4 [39,40]. However, these processes are costly and hazardous due to the required separation and treatment of spent acid, as well as the maintenance of a mitigation system, which is important in case of spillages or leakage. Several solid acid catalysts have been developed to overcome these issues, including heteropolyacids [41,42], zirconia [43,44] and zeolites as MOR [45], *BEA [44,46,47], EMT [48,49], MFI [50] and FAU [48,49,51]. Among them, 12-member ring zeolites achieved the best performances due to their larger pore sizes. Nonetheless, they lack the stability to be applied at an industrial scale. The deactivation mechanism consists of coke deposition, where the main factors influencing it are the porous structure and the acidity of the solids [52]. The first one affects the diffusion rate of coke precursors and the ease of pore blockage. The latter allows the cracking of heavy species, thus preventing coke deposition. MFI zeolites have shown poor performance in alkylation reactions, causing the dimerization reaction to prevail over alkylation. This is attributed to the impossibility of accommodating the bulkier transition state for the hydride transfer, which is the key step in the production of TMP. However, MFI zeolites present good cracking capacity, an important feature for preventing deactivation. Particularly, Peng et al. [53] showed an enhancement of 2,2,4-trimethylpentane diffusion and cracking when mesopores were incorporated into the structure of an MFI zeolite. Wodarz et al. studied the DTG conversion (gasoline from dimethyl ether) and found that mesoporous MFI presented higher gasoline selectivity and a lower deactivation rate than the parent material [24].

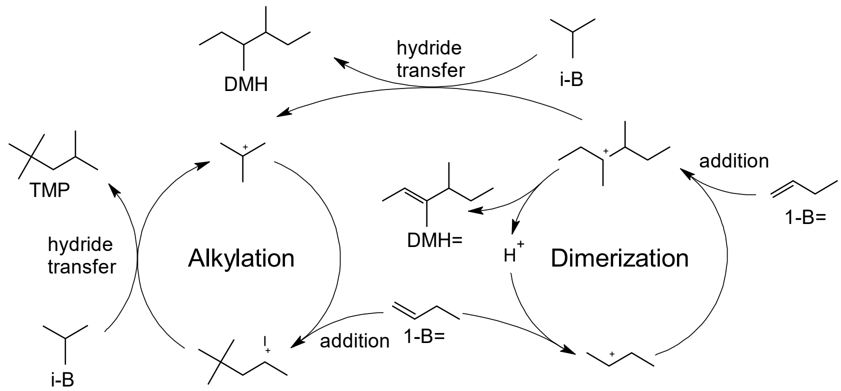

Scheme 1. Simplified representation of the reaction network of isobutane with butenes. References: isobutane (i-B), 1-butene (1-B=), trimethylpentanes (TMP), dimethylhexanes (DMH), dimethylhexenes (DMH=). (Adapted from [54] with permission form Elsevier).

In a previous work [54], the activity and accessibility of an alkaline-treated MFI zeolite (Si/Al = 15) was assessed. Since the Si/Al ratio was on the low end of feasibility for the treatment [20], harsh conditions were necessary to the development of mesoporosity. Consequentially, extensive aluminum removal occurred and acidity was greatly affected, negatively impacting the catalytic activity. In this work, a parent material with a higher Si/Al ratio (40) was employed in order to moderate the treatment conditions and better preserve the active sites. Therefore, we proposed an evaluation of the effect of the modification of the porous structure via alkaline treatment, considering the structural and acidic properties and their impact on the alkylation of isobutane with 1-butene.

The esterification of glycerol with acetic acid was also employed as a test reaction (Scheme 2). This reaction consists of three steps catalyzed by acid sites, successively yielding monoacetins (MA), diacetins (DA) and triacetin (TA). In this case, both reactants have small kinetic diameters, and they are able to penetrate the porous structure. However, their products are bulkier and present low accessibility to zeolitic structures. Therefore, studying the effect of treated catalyst on the reaction rate for each product can serve as an indicator of the accessibility of the acid sites and the characteristics of the generated mesopores.

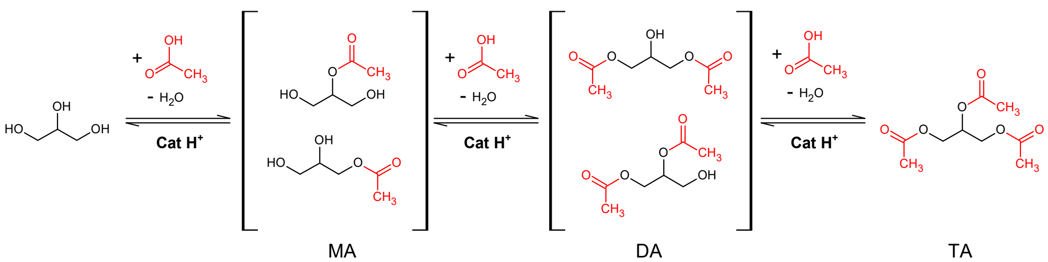

Scheme 2. Reaction mechanism for the esterification of glycerol with acetic acid.

2. Materials and Methods

Portions of a commercial MFI zeolite (CBV-8014, NH_4-form, Si/Al = 40, Zeolyst International, Conshohocken, PA USA) were exposed to aqueous NaOH (p.a., Ciccarelli, Argentina) solutions (0.05 to 1 M) at different temperatures (298, 318 and 338 K). The solution to solid ratio was 30 mL of solution per gram of zeolite. Typically, the solution was preheated to the desired temperature in a beaker in a thermostatic bath equipped with magnetic stirring, then the corresponding amount of zeolite was added and the treatment was carried out for 30 min. Then, the beaker was quenched in a 273 K water bath to stop the reaction. The solid was centrifuged, washed with distilled water several times, and then dried overnight in an oven at 353 K. In order to restore the acidity, the solid was exposed to NH_4NO_3 (p.a., Ciccarelli, Argentina) 0.5 M solution (20 mL per gram of zeolite) at 353 K under reflux for 2.5 h. It was then filtered, dried and calcined at 823 K (2 h, 1.5 K min^{-1}) under air flow. This ion exchange was repeated. Samples were labeled Z40(M/T), where M was the alkali concentration and T was the treatment temperature. Sample treated for 60 min instead of 30 were given the suffix "-1h".

For reference, a portion of the parent material (Si/Al = 40) as well as an MFI Si/Al = 15 (CBV-3020E, Valfor, Valley Forge, PA, USA) were calcined under the same conditions and labeled Z40 and Z15, respectively.

Textural properties were obtained by N_2-sorptometry using Micromeritics ASAP-2020 equipment (Norcross, GA, USA). Samples were outgassed at 523 K for 8 h, and the measurements were carried out at 77 K in the range of P/P° from 5×10^{-3} to 0.975. The surface area was estimated with the BET model. The micropore volume and external area were estimated with the t-plot method using the Harkins–Jura equation to determine the film thickness. Pore size distribution was derived from the method of Broekhoff and De Boer (BdB).

Crystallographic information was obtained by X-ray diffraction (XRD) with a Shimadzu XD-D1 device (Kyoto, Japan). Scans were performed in the range of 2θ from 5 to 60° with a speed of 2° min^{-1}. Relative values of elemental composition were obtained by X-ray fluorescence (XRF) with a Shimadzu EDX-720 in energy-dispersion mode. Samples were analyzed in a solid state.

The nature of the acid sites was studied by infrared spectroscopy (FTIR), with pyridine as a probe molecule. Samples were pressed into self-supporting wafers and placed in a cell. First, they were outgassed under a vacuum at 723 K (1 h, 10 K min^{-1}). Then, they were cooled down to 423 K and pyridine was injected. After 1 h, again, the samples were outgassed under a vacuum (1 h, 423 K). Lastly, they were cooled down to room temperature and the spectra were recorded. A JASCO FT-IR 5300 spectrometer equipped with a DTGS detector (Easton, MD, USA) was employed

The amount of acid sites in the samples and their strength profile were determined by temperature-programmed desorption of bases (TPD). Pyridine (Py) and collidine (Col) were employed as probe molecules to test the accessibility of the sites. Typically, 10 mg of sample was placed in a quartz tube and pretreated under N_2 flow (30 cm^3 min^{-1}, 1 h, 623 K, 12 K min^{-1}). Then, it was cooled down to 423 K and the catalyst bed was inundated with the liquid probe. After 30 min of contact, carrier gas was restored and the sample was purged for 1 h. Then, the analysis was carried out, which involved heating at 12 K min^{-1} to 1023 K and measuring the desorption of base with an FID (SRI Instruments, Torrance, CA, USA) coupled with a methanator for better precision. Dynamic adsorption–desorption experiments were carried out with the same setup. After the pretreatment, the sample was stabilized at 383 K and pulses of 1-butene (3 vol% in N_2) were sent every 20 s, with the outlet of the reactor connected to the detector. After a sequence of 40 pulses, a TPD was performed to quantify the amount of 1-butene remnant in the sample.

Catalytic tests for the alkylation of isobutane with butenes in gas phase were carried out in a fixed-bed reactor (5 mm i.d. × 70 mm), loaded with 200 mg of pre-sieved sample, with granulometry between 0.420 and 0.177 mm (40–80 US standard mesh). Pretreatment was carried out in situ under N_2 flow at 723 K for 1 h. The reaction mixture consisted of isobutane and 1-butene (both 99.5%, Indura, Argentina) in a ratio of 16:1. It was loaded in a pressurized tank and fed to a vaporizer at 393 K, where it was mixed with the carrier gas and fed to the reactor. The products were sampled with a multiloop valve and later analyzed with a GC (Agilent 7820A, Santa Clara, CA, USA) equipped with an FID and a ZB-1 column (100 m, Phenomenex, Torrance, CA, USA). Coke deposition after the reaction was determined by temperature-programmed oxidation (TPO) in a setup similar to TPD. The sample was loaded in a quartz cell and heated from 298 to 1023 K at 12 K min^{-1} under O_2 flow (5 vol% in N_2, 30 cm^3 min^{-1}), and the CO and CO_2 were quantified employing an FID coupled with a methanator.

The esterification of glycerol with acetic acid was tested in a batch reactor in a bath fitted with a thermostat and underwent stirring and reflux. Typically, 5 g of glycerol (99.5%, Ciccarelli, Argentina) and 200 mg of catalyst were loaded and preheated to 393 K. Then, 19.6 g of acetic acid (99.5%, Ciccarelli, Argentina) was added. The mixture was sampled at regular intervals for GC analyses, which employed an HP-FFAP column (30 m, Agilent, Santa Clara, CA, USA).

3. Results

3.1. Evaluation of Treatment Conditions

A screening of treatment conditions was conducted. The alkali concentration varied between 0.05 and 0.7 M and the temperature varied between 25 and 65 °C. For the most advantageous condition, an additional test was carried out, extending the duration to 1 h. The textural properties and Si/Al ratios are shown in Table 1, while the most representative results are represented in Figure 1.

Table 1. Textural properties and Si/Al ratios of treated zeolites.

Material	Surface Area (m^2 g^{-1})		Pore Volume (cm^3 g^{-1})			Si/Al (mol/mol)
	S_{BET}	External	Total	Microp.	Mesop.	
Z40	430	44	0.231	0.166	0.065	40.55
Z40(0.05/25)	394	63	0.226	0.137	0.089	41.02
Z40(0.1/25)	379	50	0.218	0.135	0.083	39.62
Z40(0.2/25)	384	47	0.221	0.138	0.083	42.27
Z40(0.5/25)	389	50	0.222	0.137	0.085	41.00
Z40(0.1/45)	425	91	0.263	0.140	0.123	41.13
Z40(0.2/45)	407	91	0.271	0.143	0.129	33.55
Z40(0.5/45)	432	141	0.332	0.122	0.209	25.93
Z40(0.7/45)	375	84	0.368	0.118	0.250	25.40
Z40(0.1/65)	424	88	0.274	0.142	0.132	35.25
Z40(0.2/65)	492	177	0.496	0.110	0.385	33.39
Z40(0.3/65)	500	240	0.745	0.117	0.627	25.21
Z40(0.5/65)	441	239	0.806	0.090	0.717	8.51
Z40(0.7/65)	254	172	0.609	0.036	0.573	4.88
Z40(0.5/45)-1h	408	103	0.567	0.122	0.445	17.71
Z15	370	37	0.198	0.139	0.059	15.04

The treatment at 25 °C was ineffective and no significant mesoporosity was obtained. The development of mesoporosity (by surface and volume) was observed from 45 °C. This was enhanced at 65 °C, but was accompanied by a decrement in micropore volume. Furthermore, the optimum alkali concentration required to generate mesopores was found to be between 0.2 and 0.5 M. Treatment with 0.7 M solution was detrimental for both the generation of mesopores as well as the preservation of preexistent micropores.

Figure 2 shows the pore size distributions obtained by the BdB method. Treatments conducted at 25 °C resulted in a poor development of porosity, displaying narrow distributions centered around 9 nm. Conversely, treatments at 65 °C had a strong impact on the framework, leading to broader distributions, which were characterized by a main peak centered between 20 and 30 nm accompanied by a secondary peak between 10 and 15 nm. Moreover, a loss of material between 75 and 95% was observed during the treatment, indicating the collapse of the framework.

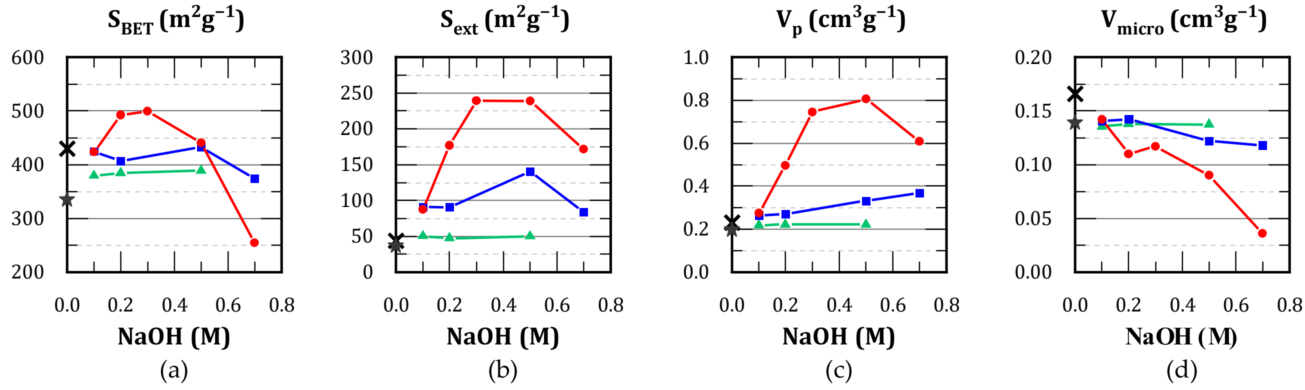

Figure 1. Influence of alkali concentration on representative textural properties at different temperatures: 25 °C (▲), 45 °C (■), and 65 °C (●). For reference, zeolites Z15 (★) and Z40 (✖) are shown as well. (**a**) BET surface area; (**b**) external surface area; (**c**) total pore volume; (**d**) micropore volume.

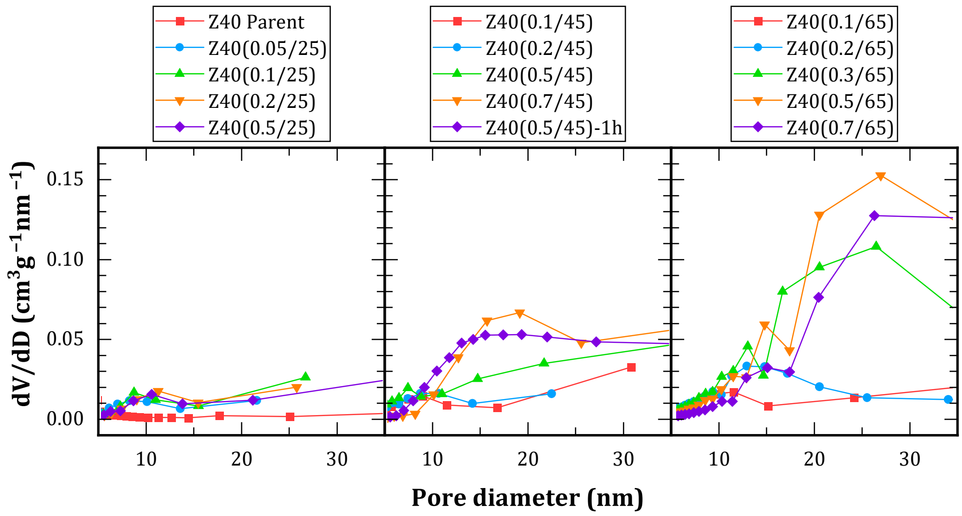

Figure 2. Pore size distributions determined by the BdB method from N_2 sorptometry, grouped by treatment temperature.

Treatments conducted at 45 °C were more moderate, leading to a loss of between 45 and 85% of the initial solid. Among them, Z40(0.7/45) and Z40(0.5/45)-1h had the most uniform pore size distributions.

When comparing Z40(0.5/45) and Z40(0.5/45)-1h, it can be seen that the extended treatment time led to a consistent reduction in the Si/Al ratio (about 40% for every 30 min). This was accompanied by an increment in mesopore volume, without a notable decrement in micropore volume but with a decrement in mesopore area. This would indicate a broadening of the pores, consistent with the distributions shown in Figure 2. Moreover, the loss of solid increased from 45% to 67%.

In general, increments in treatment duration led to pore broadening. The same effect was observed for the alkali concentration, but was more pronounced. When comparing Z40(0.7/45) and Z40(0.5/45)-1h, the latter presented an 80% higher pore volume but only 22% higher surface area. The Si/Al ratio is much lower for the latter, indicating a higher desilication. The temperature of the treatment represents a compromise between selectivity for silicon removal and the overall kinetics. Higher temperatures accelerate the generation of mesopores, but they also lead to aluminum removal.

After the alkaline treatments, the acidity of the materials was restored via a cationic exchange with NH_4NO_3 in order to recover their catalytic properties. Table 2 shows the results for selected materials. Experimental XRD patterns can be found in the Supplementary Material (Figure S1). For comparative purposes, theoretical amounts of acid sites were estimated as a function of the Si/Al ratio. The canonic unit cell for the MFI framework obeys the formula $H_nAl_nSi_{96-n}O_{192}{\cdot}16H_2O$. For every n, the Si/Al ratio is (96−n)/n and the amount of acid sites (in mmol g^{-1}) is equal to 1000 n/PM(n), where PM(n) is the formula weight of the unit cell in g mol^{-1}, since it is assumed that every framework, Al provides one acid site. This theoretical curve was generated for n between 2 and 30 and plotted in Figure 3, together with the values reported for the treated materials in Table 2.

Table 2. Acidic properties of selected materials.

Material	Cristallinity (%)	Acid Sites [a] (mmol g^{-1})	Brønsted Acid sites [b] (%)	External Acid Sites [c] (mmol g^{-1})
Z40	100	0.39	80.6	0.10
Z40(0.5/45)	56.0	0.77	69.6	0.27
Z40(0.7/45)	69.0	0.96	75.4	n. d.
Z40(0.1/65)	67.5	0.69	76.9	n. d.
Z40(0.2/65)	88.9	0.58	n. d.	n. d.
Z40(0.3/65)	79.9	0.69	n. d.	n. d.
Z40(0.5/65)	40.8	0.70	n. d.	n. d.
Z40(0.7/65)	22.8	0.44	n. d.	n. d.
Z40(0.5/45)-1h	35.3	1.35	67.3	0.31
Z15	100	1.44	81.0	0.23

[a] Determined by pyridine TPD. [b] Determined by pyridine FTIR. [c] Determined by collidine TPD. n. d.—not determined.

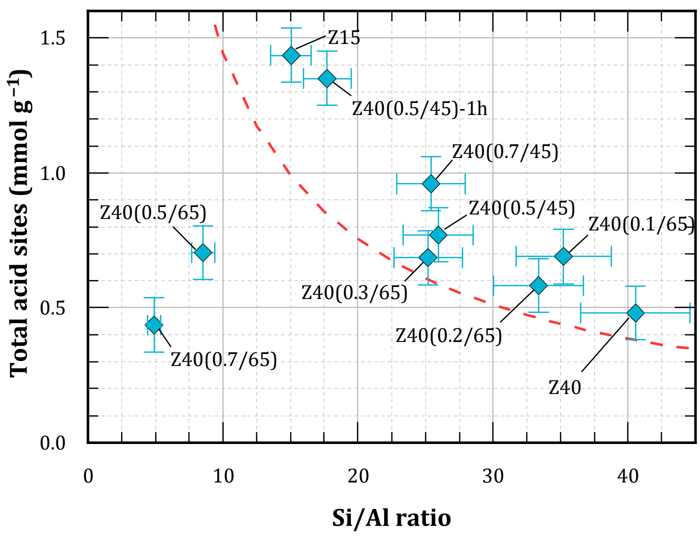

Figure 3. Amount of acid sites vs. Si/Al ratio for selected materials. Theoretical relationship indicated by the dashed line.

From Figure 3, it can be seen that non-treated zeolites, as well as those subjected to moderate treatment, lie above the theoretical curve. This can be attributted to the presence of framework defects, as well as extra-framework aluminum (EFAL) species. On the other hand, the solids obtained after more severe treatments exhibit lower amounts of acid sites compared with the theoretical curve. Presumably, this is due to the loss of the structure and partial framework collapse, consistent with the cristallinity values obtained by XRD.

3.2. Evaluation of the Accessibility of the Acid Sites

The location and accessibility of the acid sites were studied in order to correlate the catalytic performance with the amount of acid sites and the development of mesoporosity. Two probe molecules were employed for that purpose: pyridine (Py) and collidine (Col). Py has a kinetic diameter of about 5.4 Å and is just small enough to diffuse through the micropores of MFI zeolites. Col (2,4,6-trimethylpyridine) has a bigger kinetic diameter (7.4 Å); therefore, it can diffuse through mesopores, but it is not able to enter the micropores of the zeolites. The TPD profiles of both probe molecules are presented in Figure 4. The integration of these profiles results in the amounts of acid sites included in Table 2, where Py-TPD corresponds to total acid sites and Col-TPD to external acid sites (i.e., those located in the mesopores and the outer area of the particles).

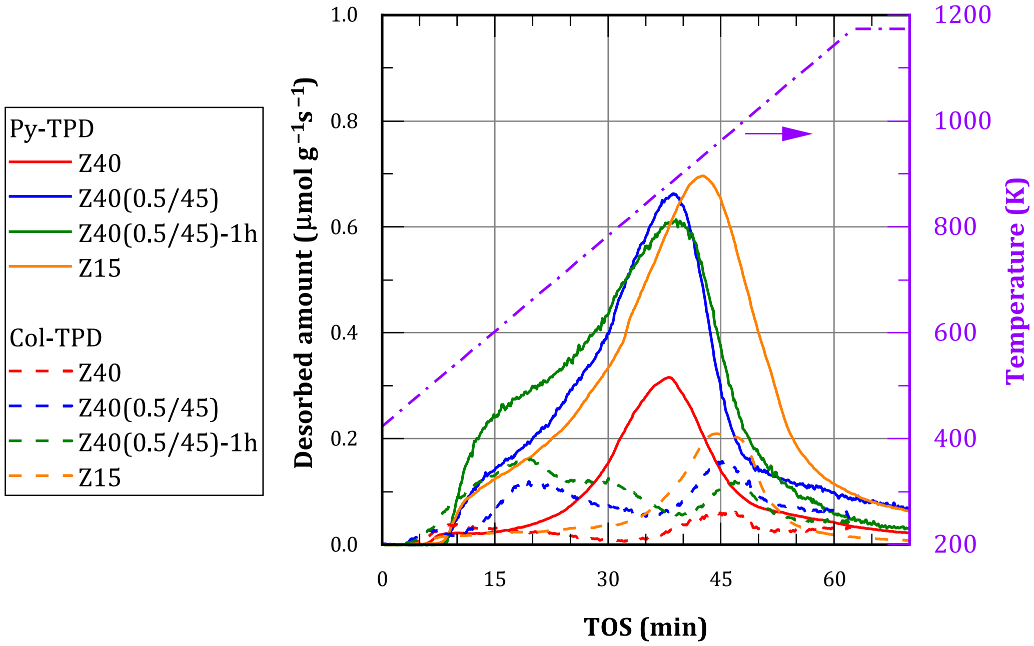

Figure 4. TPD profiles obtained using pyridine (Py) and collidine (Col) as probe molecules.

Py-TPD profiles were found to be similar in shape, with different magnitudes, in correspondence with changes in the Si/Al ratio. Strong acid sites predominate, with a maximum between 850 and 950 K. There were also a considerable number of moderate acid sites, seen as a shoulder of the main peak with a center in the range 650–750 K. Finally, there are weak acid sites, associated with a desorption maxima below 550 K.

Since desilication decreases Si/Al ratio and leads to an increment in the amount of acid sites, in order to assess how the treatment affected the acidity, Z40(0.5/45)-1h was compared with commercial zeolite Z15. Therefore, it was observed that the treated material exhibited a higher proportion of moderate sites and fewer strong sites. The desorption peak shifted to lower temperatures for Z40(0.5/45)-1h, indicating that sites in Z15 are stronger.

Col-TPD profiles showed that the alkaline treatment increased the amount of accessible acid sites. Though most of these were weakly or moderately acidic sites, the amount of accessible strong sites increased as well. The number of accessible sites in treated zeolites was higher than the number of sites found in Z15, but the latter are predominantly strong.

The density of external acid sites was computed as the quotient between the amount of acid sites accessible to Col and the external area (Table 2). This value was diminished after alkaline treatment due to the superposition of two factors: (i) The alkali attacked the surface, affecting its crystallinity and leaching some isolated Al atoms. (ii) The external area increased with the generation of mesopores. Therefore, it can be concluded that the generated mesopores provide additional external area, but the amount of strong acid sites present is insignificant.

The nature of the acid sites was further explored by infrared spectroscopy. Figure 5a shows the spectra of the activated samples in the OH region. The alkaline treatment leads to a rise in the bands associated with terminal silanols (3740 cm^{-1}) and nested silanols (3725 cm^{-1}), as well as the appearance of a small signal at 3680 cm^{-1}, which is associated with EFAL [55]. Therefore, desilication treatment leads to an increment in defect sites, as well as limited removal of Al atoms, which later deposit as extra-framework species. The spectra after pyridine adsorption and outgassing are shown in Figure 5b. The bands associated with Brønsted acid sites (1635 and 1545 cm^{-1}) are more intense for treated materials than the parent zeolite (Z40), but not as intense as Z15. On the other hand, the bands associated with Lewis acid sites (1624 and 1455 cm^{-1}) increase sharply in treated materials, and are more intense than those of Z15. The results of quantification, based on the bands located at 1545 and 1455 cm^{-1} are included in Table 2. Since Lewis acid sites increase more markedly than Brønsted acid sites, the overall result is a decrement in the proportion of the latter, from around 80% in parent material to less than 70% in treated materials Z40(0.5/45) and Z40(0.5/45)-1h. These sites are detrimental for the catalytic activity, for multiple reasons [56,57]: (i) They do not catalyze the alkylation reaction, since the key step involves protonation, which requires strong Brønsted acid sites. (ii) They lead to the formation of unsaturated compounds and their oligomerization. (iii) This ultimately favors coke deposition and deactivation of neighboring Brønsted acid sites.

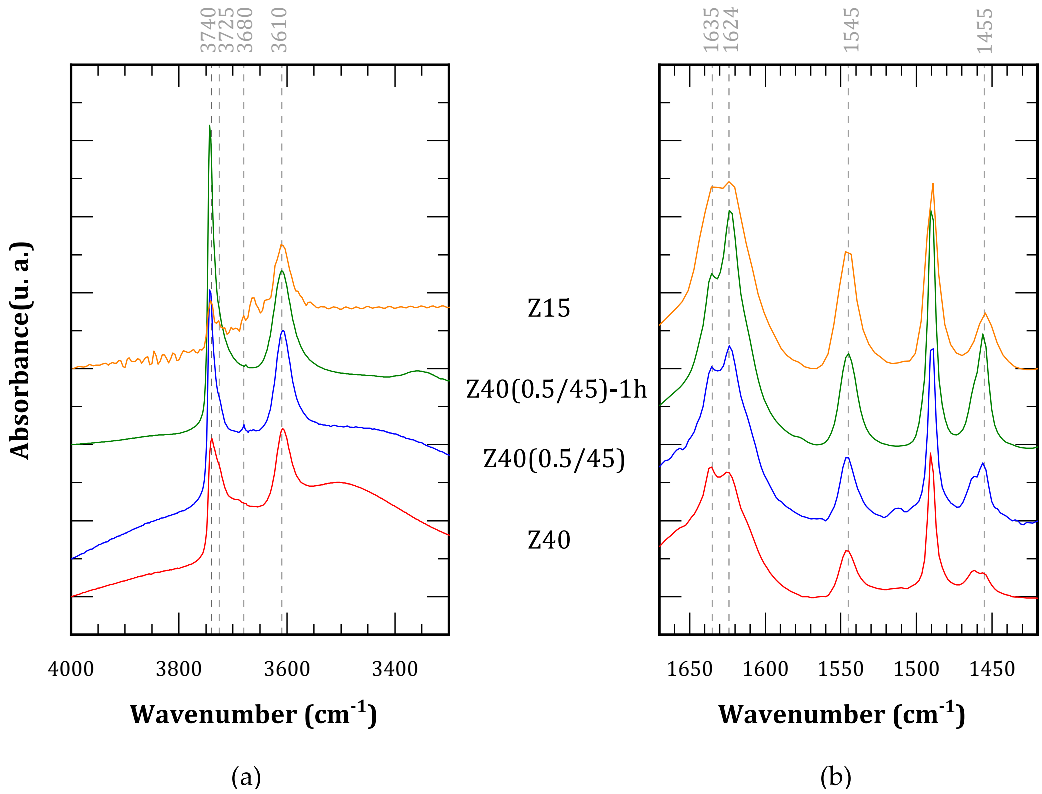

Figure 5. FTIR spectra in regions of interest: (**a**) after activation; (**b**) after pyridine adsorption.

3.3. Dynamic Adsorption Experiments

The interaction of the solid with one reactant (1-butene) was analyzed by dynamic adsorption. The experiments consisted of trains of pulses of 1-butene sent to a cell at 110 °C loaded with catalyst, while the outlet was monitored by FID. The results are presented in Figure 6. Z40 adsorbs the pulses completely for the first 200 s, and then reduces the uptake until saturation. Z40(0.5/45) and Z40(0.5/45)-1h adsorb 1-butene more slowly, indicating comparatively weaker acid sites. This corroborates previous results [54,58]. Once stabilized, the amplitude of the peaks is lower than the blank test due to a widening caused by the diffusion of the reactant through the solid. The integration of the profiles shows that Z40 adsorbed 3.56 mmol of butene per gram of solid, while Z40(0.5/45) and Z40(0.5/45)-1h adsorbed 1.93 and 1.99 mmol g^{-1}, respectively.

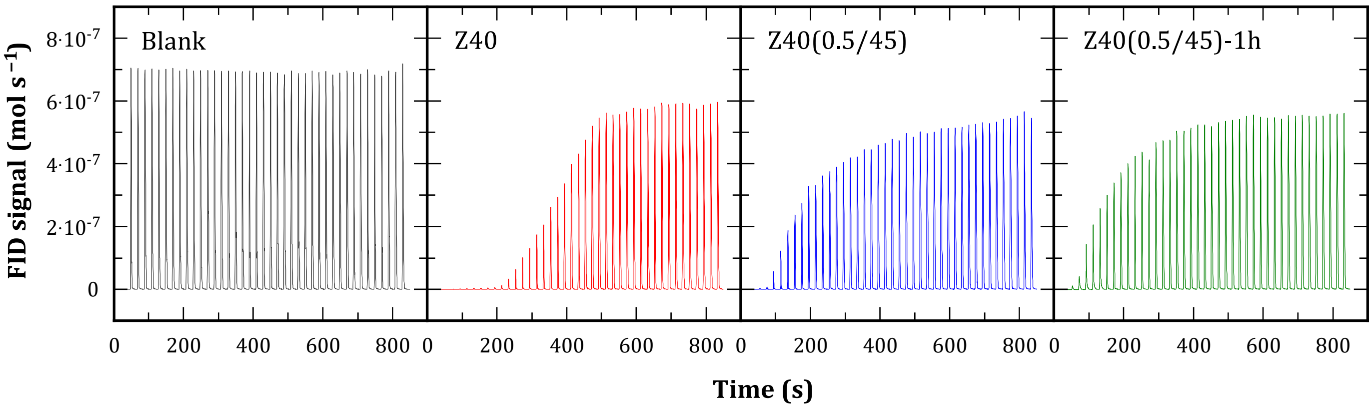

Figure 6. Pulses of 1-butene over different catalysts.

After the equilibration of the catalyst with 1-butene, a TPD was performed, yielding the profiles shown in Figure 7. Their three main contributions are presented as follows:

- The first contribution is 425–450 K: butenes, which enable the isomerization of 1-butene.
- The second contribution is 450–525 K: light olefins, which result from polymerization reactions.
- The third contribution is 500–575 K: species released from coke, coinciding with those typically observed in TPO experiments.

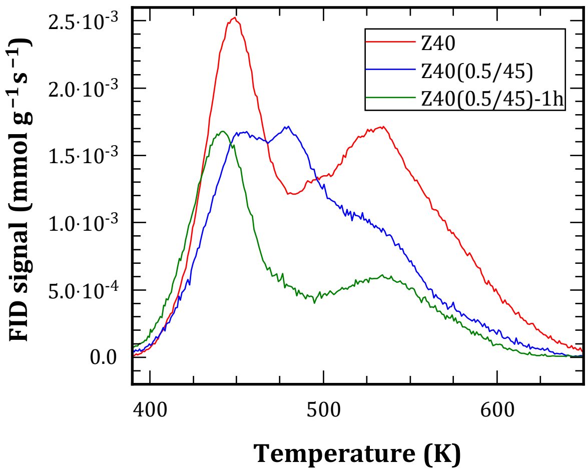

Figure 7. TPD profiles after pulses of 1-butene.

The total desorbed species represented between 30 and 50% of the adsorbed 1-butene considering the carbon atoms. This indicates that coke on the solids, and was not released due to the use of N_2 as carrier gas.

Regarding the profiles, treated materials were less acidic; thus, they adsorbed less 1-butene and, consequently, presented smaller amounts of desorption as well. In relative terms, the high-temperature contribution was reduced. This can be attributed to a lower ability to crack the coke precursors due to their weaker acid sites.

3.4. Catalytic Evaluation

3.4.1. Isobutane/1-Butene Alkylation

The catalysts were tested for the alkylation of isobutane with butenes in the gas phase. Although 1-butene was employed as a reactant here, it can undergo rapid isomerization to cis- and trans-2-butene. Both isomers were detected among the products, and therefore they can act as alkylating agents.

The results of butenes' conversion to and selectivity for different hydrocarbon fractions as a function of time on stream (TOS) are shown in Figure 8. All catalysts presented a reduction in conversion with TOS due to deactivation caused by coke deposition. However, the treated catalysts showed delayed deactivation and higher residual activity after deactivation. This behavior is attributed to their mesoporous structure, which facilitated the diffusion of coke precursors, as well as preventing pore-mouth blocking by providing alternate routes for reactants and products. Z40(0.5/45) also provided a higher initial conversion (over 90%), indicating a good proportion of strong acid sites. This material presented lower coke deposition at the end of the reaction, likely due to the enhanced diffusion of coke precursors. Z40(0.5/45)-1h presented intermediate behavior between the latter and the parent zeolite, indicating that the extension of the alkaline treatment was detrimental for the catalytic activity.

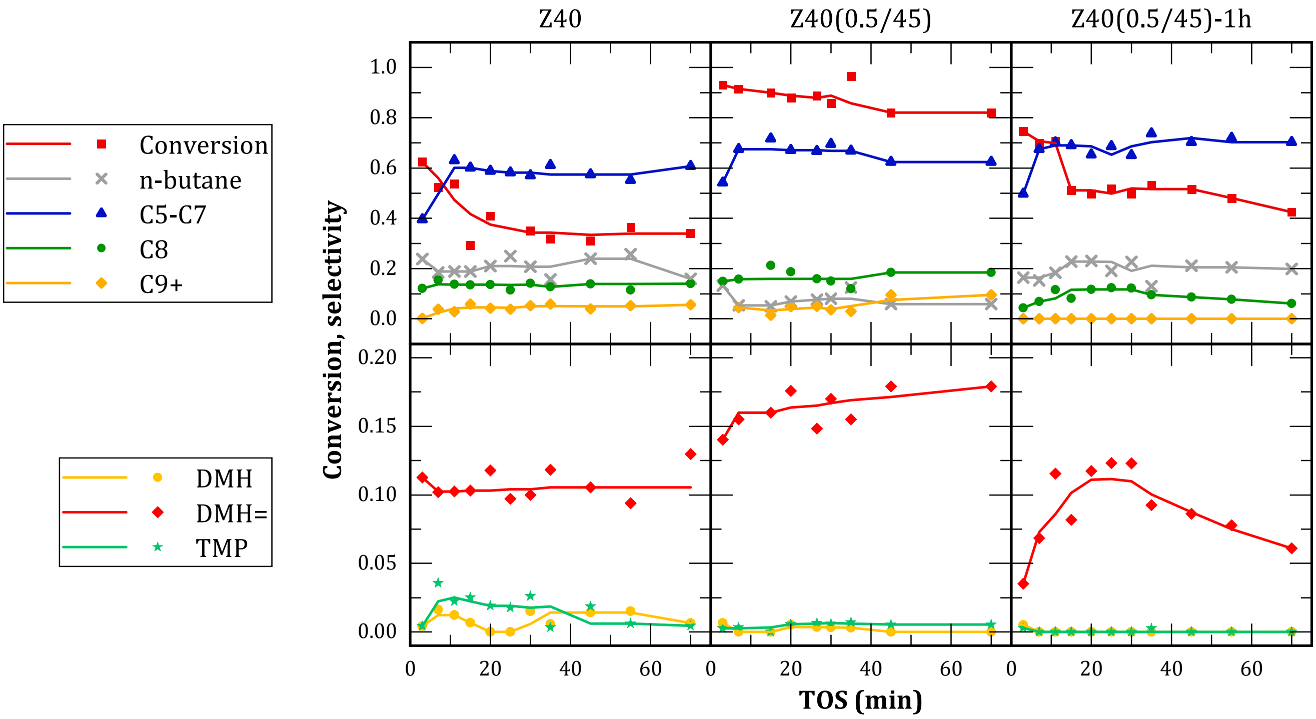

Figure 8. Butene conversion and selectivity to different hydrocarbon fractions. Selectivity to components of the C8 fraction is shown in detail: dimethylhexanes (DMH), dimethylhexenes (DMH=) and trimethylpentanes (TMP).

MFI zeolites have been previously studied with regard to this reaction, resulting in low yields to trimethylpentanes (TMP) due to their channel structure [45]. In this case, it is observed that the selectivity of the parent zeolite is replicated by the treated catalysts. In the C5+ fraction, there is a predominance of C5–C7 products, which is formed by oligomerization followed by cracking. Approximately 10–20% of C8 compounds were obtained, almost entirely DMH=. The presence of these compounds suggests a predominance of butene dimerization and a low hydride transfer activity. The observed DMH= compounds are responsible for the formation of C9+ hydrocarbons, which act as coke precursors.

As mentioned above, the microporous channels in MFI zeolites impose steric hindrances that limit the formation of multibranched compounds. Consequently, Z40 was more selective towards dimerization and polymerization reactions, while the formation of TMP was hindered. Treated materials presented similar product distributions; therefore, the mesopores did not appear to contribute to the formation of TMP. These results suggest, in agreement with accessibility tests, that the mesopores generated by alkaline treatment do not have active sites for this reaction on their surface. These results agree with those obtained by Sazama et al. [59], who studied n-hexane isomerization and found that shape selectivity in zeolites was not affected by secondary mesoporosity.

The parent material Z40 produced the highest proportion of TMP, which is attributed to the presence of accessible strong sites located at the pore mouths. After the alkaline treatment, these sites close to the external surface were attacked and consequently lost. The remaining accessible sites were weak and, presumably, Lewis acid sites associated with EFAL originated by redeposition of removed aluminum.

TPO profiles (Figure 9) presented two distinctive regions corresponding to aliphatic coke (300–650 K) and aromatic coke (650–1000 K). The latter was produced by an aromatization process during the analysis [52], and it represents a minor contribution to the profile. Higher amounts indicate the presence of strong acid sites and a more efficient use of the catalyst surface, as observed in FAU zeolites [60].

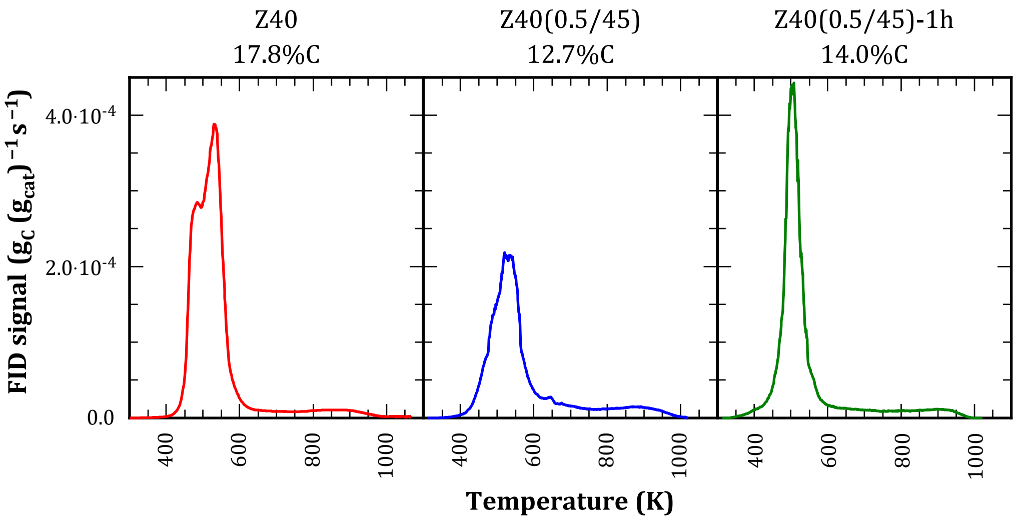

Figure 9. TPO profiles for the catalysts after one reaction cycle. The total amount of coke is indicated next to each graph.

3.4.2. Glycerol Esterification with Acetic Acid

The catalysts were also tested for the esterification of glycerol with acetic acid to obtain mono-, di- and triacetin (MA, DA and TA, respectively). This reaction takes place under different conditions than the alkylation reaction (liquid phase, polar reactants) but also requires acid sites and large pores due to the increasing kinetic diameter of the successive products. Therefore, a contrast is provided regarding the effect of the alkaline treatment and the generation of mesopores.

Glycerol's conversion and selectivities to MA, DA and TA are shown in Figure 10 for the catalysts and the blank test, since there is an intrinsic reaction rate between the reactant in the absence of catalyst. As a comparison, the reaction with a homogeneous strong acid (p-toluenesulfonic acid, PTSA) is provided.

The blank test achieved 90% glycerol conversion after 4 h, yielding predominantly MA. After 6 h, the DA selectivity was 50% and TA, 10%. PTSA (added in a quantity equivalent to the acid sites of the average of the solids) reached 90% glycerol conversion in 1 h and selectivities equilibrated after 6 h, with the proportion of MA:DA:TA being around 23:55:22.

Solid catalysts reported similar yields to the blank test. In particular, higher initial reaction rates were observed and the crossing point of MA and DA selectivities shifted to lower reaction times. TA selectivity curves did not present significant changes. Overall, this would indicate a catalytic effect on the first stage of the reaction, with some effect on the second stage by equilibrium displacement.

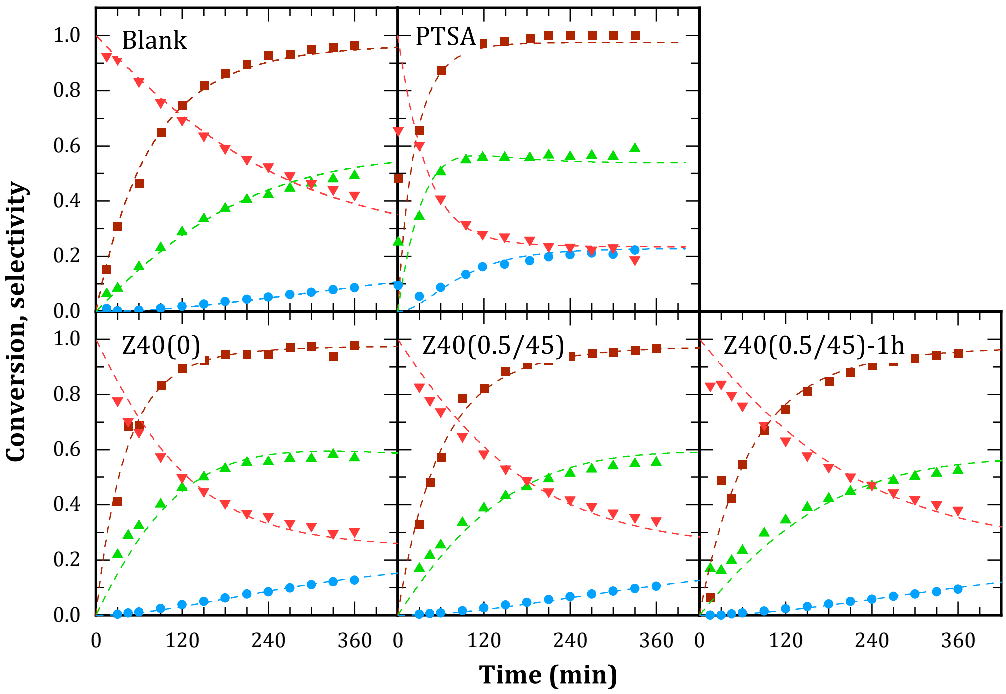

Figure 10. Glycerol conversion (■) and selectivity to MA (▼), DA (▲) and TA (•) for the blank test and for different catalysts.

4. Discussion

The generation of mesopores by alkaline treatment, while preserving parent material crystallinity, is only possible within narrow ranges of alkali concentration and temperature, and with a limited duration. Under adequate conditions, pores with diameters around 10 nm were formed, and mesopore volume increased by 300%. The amount of acid sites increased due to selective removal of silicon atoms. Nonetheless, desorption of bases of different kinetic diameters revealed that these mesopores lack active sites on their surface, which are partially amorphized due to alkali attack. Additionally, some aluminum is incidentally removed during treatment and redeposits in the mesopores as EFAL, originating accessible weak Lewis acid sites.

The lack of moderate and strong Brønsted acid sites in the mesopores confines catalytic activity to preexisting micropores. Therefore, shape selectivity of the parent zeolite is preserved in treated materials, as was demonstrated for the alkylation of isobutane with butenes. Pore sizes play a key role in selectivity to different C8 products in this reaction, and the materials yielded only dimerization products, since they could not accommodate the bulky intermediate state required for the hydride transfer. This conclusion was further supported by the study of esterification of glycerol with acetic acid, where the solids lacked catalytic activity due to steric hindrances in the micropores. However, in the first case, the existence of mesopores allowed better diffusion of coke precursors. Therefore, coke deposition was delayed, pore blocking was avoided, and catalytic activity was preserved, increasing the stability of the catalyst for the alkylation reaction system.

Supplementary Materials: The following supporting information can be downloaded at https://www.mdpi.com/article/10.3390/pr12112567/s1, Figure S1. XRD Patterns of selected alkaline-treated MFI zeolites and the parent material.

Author Contributions: Conceptualization, L.G.T. and B.O.D.C.; methodology, L.G.T.; formal analysis, L.G.T., L.V., B.O.D.C. and C.A.Q.; investigation, L.G.T. and L.V.; resources, B.O.D.C. and C.A.Q.; data curation, L.G.T.; writing—original draft preparation, L.G.T.; writing—review and editing, B.O.D.C.; visualization, L.G.T.; supervision, C.A.Q.; project administration, B.O.D.C. and C.A.Q.; funding acquisition, B.O.D.C. and C.A.Q. All authors have read and agreed to the published version of the manuscript.

Funding: This research was funded by ANPCyT, project PICT 2018-0364; CONICET project PIP 2022-0345; and Universidad Nacional del Litoral, project CAI+D 2020 50620190100153LI.

Data Availability Statement: Dataset available on request from the authors.

Conflicts of Interest: The authors declare no conflicts of interest.

References

1. Bai, R.; Song, Y.; Li, Y.; Yu, J. Creating Hierarchical Pores in Zeolite Catalysts. *Trends Chem.* **2019**, *1*, 601–611. [CrossRef]
2. Serrano, D.P.; Escola, J.M.; Pizarro, P. Synthesis Strategies in the Search for Hierarchical Zeolites. *Chem. Soc. Rev.* **2013**, *42*, 4004–4035. [CrossRef]
3. Schwieger, W.; Machoke, A.G.; Weissenberger, T.; Inayat, A.; Selvam, T.; Klumpp, M.; Inayat, A. Hierarchy Concepts: Classification and Preparation Strategies for Zeolite Containing Materials with Hierarchical Porosity. *Chem. Soc. Rev.* **2016**, *45*, 3353–3376. [CrossRef]
4. Tzoulaki, D.; Jentys, A.; Pérez-Ramírez, J.; Egeblad, K.; Lercher, J.A. On the Location, Strength and Accessibility of Bronsted Acid Sites in Hierarchical ZSM-5 Particles. *Catal. Today* **2012**, *198*, 3–11. [CrossRef]
5. Rownaghi, A.A.; Hedlund, J. Methanol to Gasoline-Range Hydrocarbons: Influence of Nanocrystal Size and Mesoporosity on Catalytic Performance and Product Distribution of ZSM-5. *Ind. Eng. Chem. Res.* **2011**, *50*, 11872–11878. [CrossRef]
6. Airi, A.; Signorile, M.; Bonino, F.; Quagliotto, P.; Bordiga, S.; Martens, J.A.; Crocellà, V. Insights on a Hierarchical MFI Zeolite: A Combined Spectroscopic and Catalytic Approach for Exploring the Multilevel Porous System down to the Active Sites. *ACS Appl. Mater. Interfaces* **2021**, *13*, 49114–49127. [CrossRef]
7. Sammoury, H.; Toufaily, J.; Cherry, K.; Hamieh, T.; Pouilloux, Y.; Pinard, L. Desilication of *BEA Zeolites Using Different Alkaline Media: Impact on Catalytic Cracking of n-Hexane. *Microporous Mesoporous Mater.* **2018**, *267*, 150–163. [CrossRef]
8. Fathi, S.; Sohrabi, M.; Falamaki, C. Improvement of HZSM-5 Performance by Alkaline Treatments: Comparative Catalytic Study in the MTG Reactions. *Fuel* **2014**, *116*, 529–537. [CrossRef]
9. Lima, R.B.; Neto, M.M.S.; Oliveira, D.S.; Santos, A.G.D.; Souza, L.D.; Caldeira, V.P.S. Obtainment of Hierarchical ZSM-5 Zeolites by Alkaline Treatment for the Polyethylene Catalytic Cracking. *Adv. Powder Technol.* **2021**, *32*, 515–523. [CrossRef]
10. Ma, Q.; Fu, T.; Li, H.; Cui, L.; Li, Z. Insight into the Selection of the Post-Treatment Strategy for ZSM-5 Zeolites for the Improvement of Catalytic Stability in the Conversion of Methanol to Hydrocarbons. *Ind. Eng. Chem. Res.* **2020**, *59*, 11125–11138. [CrossRef]
11. Rodrigues, M.V.; Vignatti, C.; Garetto, T.; Pulcinelli, S.H.; Santilli, C.V.; Martins, L. Glycerol Dehydration Catalyzed by MWW Zeolites and the Changes in the Catalyst Deactivation Caused by Porosity Modification. *Appl. Catal. A Gen.* **2015**, *495*, 84–91. [CrossRef]
12. Mardiana, S.; Azhari, N.J.; Ilmi, T.; Kadja, G.T.M. Hierarchical Zeolite for Biomass Conversion to Biofuel: A Review. *Fuel* **2022**, *309*, 122119. [CrossRef]
13. Peron, D.V.; Zholobenko, V.L.; de Melo, J.H.S.; Capron, M.; Nuns, N.; de Souza, M.O.; Feris, L.A.; Marcilio, N.R.; Ordomsky, V.V.; Khodakov, A.Y. External Surface Phenomena in Dealumination and Desilication of Large Single Crystals of ZSM-5 Zeolite Synthesized from a Sustainable Source. *Microporous Mesoporous Mater.* **2019**, *286*, 57–64. [CrossRef]
14. Kortunov, P.; Vasenkov, S.; Kärger, J.; Valiullin, R.; Gottschalk, P.; Elía, M.F.; Perez, M.; Stöcker, M.; Drescher, B.; McElhiney, G.; et al. The Role of Mesopores in Intracrystalline Transport in USY Zeolite: PFG NMR Diffusion Study on Various Length Scales. *J. Am. Chem. Soc.* **2005**, *127*, 13055–13059. [CrossRef]
15. Okamoto, G.; Okura, T.; Goto, K. Properties of Silica in Water. *Geochim. Cosmochim. Acta* **1957**, *12*, 123–132. [CrossRef]
16. Iler, R.K. *The Chemistry of Silica: Solubility, Polymerization, Colloid and Surface Properties and Biochemistry of Silica*; Wiley: New York, NY, USA, 1979; ISBN 978-0-471-02404-0.
17. Dessau, R.M.; Valyocsik, E.W.; Goeke, N.H. Aluminum Zoning in ZSM-5 as Revealed by Selective Silica Removal. *Zeolites* **1992**, *12*, 776–779. [CrossRef]
18. Svelle, S.; Sommer, L.; Barbera, K.; Vennestrøm, P.N.R.; Olsbye, U.; Lillerud, K.P.; Bordiga, S.; Pan, Y.H.; Beato, P. How Defects and Crystal Morphology Control the Effects of Desilication. *Catal. Today* **2011**, *168*, 38–47. [CrossRef]
19. Ogura, M.; Shinomiya, S.Y.; Tateno, J.; Nara, Y.; Kikuchi, E.; Matsukata, M. Formation of Uniform Mesopores in ZSM-5 Zeolite through Treatment in Alkaline Solution. *Chem. Lett.* **2000**, *29*, 882–883. [CrossRef]
20. Groen, J.C.; Jansen, J.C.; Moulijn, J.A.; Pérez-Ramírez, J. Optimal Aluminum-Assisted Mesoporosity Development in MFI Zeolites by Desilication. *J. Phys. Chem. B* **2004**, *108*, 13062–13065. [CrossRef]
21. Groen, J.C.; Moulijn, J.A.; Pérez-Ramírez, J. Alkaline Posttreatment of MFI Zeolites. From Accelerated Screening to Scale-Up. *Ind. Eng. Chem. Res.* **2007**, *46*, 4193–4201. [CrossRef]
22. Groen, J.C.; Moulijn, J.A.; Pérez-Ramírez, J. Decoupling Mesoporosity Formation and Acidity Modification in ZSM-5 Zeolites by Sequential Desilication-Dealumination. *Microporous Mesoporous Mater.* **2005**, *87*, 153–161. [CrossRef]
23. Verboekend, D.; Mitchell, S.; Milina, M.; Groen, J.C.; Pérez-Ramírez, J. Full Compositional Flexibility in the Preparation of Mesoporous MFI Zeolites by Desilication. *J. Phys. Chem. C* **2011**, *115*, 14193–14203. [CrossRef]
24. Wodarz, S.; Slaby, N.A.; Zimmermann, M.C.; Otto, T.N.; Holzinger, J.; Skibsted, J.; Zevaco, T.A.; Pitter, S.; Sauer, J. Shaped Hierarchical H-ZSM-5 Catalysts for the Conversion of Dimethyl Ether to Gasoline. *Ind. Eng. Chem. Res.* **2020**, *59*, 17689–17707. [CrossRef]

25. Gu, J.; Lin, J.; Smith, A.J.; Soontaranon, S.; Rugmai, S.; Kongmark, C.; Coppens, M.O.; Sankar, G. Towards Understanding Mesopore Formation in Zeolite Y Crystals Using Alkaline Additives via in Situ Small-Angle X-Ray Scattering. *Microporous Mesoporous Mater.* **2022**, *338*, 111867. [CrossRef]
26. Zhang, H.; Wang, L.; Xie, Y.; Zhang, S.; Ning, P.; Wang, X. Tailoring Mesoporosity and Acid Sites for Enhanced Gaseous As_2O_3 Adsorption by Alkaline-Etching ZSM-5 with Different Si/Al Ratios. *Sep. Purif. Technol.* **2025**, *354*, 129081. [CrossRef]
27. Shahid, A.; Inayat, A.; Avadhut, Y.; Hartmann, M.; Schwieger, W. A Comparative Study of the Desilication of Channel- and Cage-like Zeolites. *Microporous Mesoporous Mater.* **2022**, *341*, 111903. [CrossRef]
28. Li, X.; Hernandez Gaitan, J.A.; Kokuryo, S.; Sumi, T.; Kitamura, H.; Miyake, K.; Uchida, Y.; Nishiyama, N. Hierarchical Zeolites with High Hydrothermal Stability Prepared via Desilication of OSDA-Occluded Zeolites. *Microporous Mesoporous Mater.* **2022**, *344*, 112096. [CrossRef]
29. Wang, Z.; Zhang, R.; Wang, J.; Yu, Z.; Xiang, Y.; Kong, L.; Liu, H.; Ma, A. Hierarchical Zeolites Obtained by Alkaline Treatment for Enhanced N-Pentane Catalytic Cracking. *Fuel* **2022**, *313*, 122669. [CrossRef]
30. Abelló, S.; Bonilla, A.; Pérez-Ramírez, J. Mesoporous ZSM-5 Zeolite Catalysts Prepared by Desilication with Organic Hydroxides and Comparison with NaOH Leaching. *Appl. Catal. A Gen.* **2009**, *364*, 191–198. [CrossRef]
31. Wang, P.; Chen, T.; Qiu, Z.; Yao, W.; Liu, P.; Zhang, Y.; Song, Y.; Cui, Q.; Bao, X. Pt-Promoted Mesoporous Beta Zeolite Catalysts for n-Hexane Isomerization with Enhanced Selectivity to Dibranched Isomers. *Fuel* **2024**, *368*, 131593. [CrossRef]
32. Pyra, K.; Tarach, K.A.; Majda, D.; Góra-Marek, K. Desilicated Zeolite BEA for the Catalytic Cracking of LDPE: The Interplay between Acidic Sites' Strength and Accessibility. *Catal. Sci. Technol.* **2019**, *9*, 1794–1801. [CrossRef]
33. Verboekend, D.; Vilé, G.; Pérez-Ramírez, J. Mesopore Formation in Usy and Beta Zeolites by Base Leaching: Selection Criteria and Optimization of Pore-Directing Agents. *Cryst. Growth Des.* **2012**, *12*, 3123–3132. [CrossRef]
34. Feng, Y.; Xiao, X.M.; Wang, E.Z.; Gao, P.; Lu, C.G.; Li, G. Gas Storage in Shale Pore System: A Review of the Mechanism, Control and Assessment. *Pet. Sci.* **2023**, *20*, 2605–2636. [CrossRef]
35. Ehlinger, V.M.; Gabriel, K.J.; Noureldin, M.M.B.; El-Halwagi, M.M. Process Design and Integration of Shale Gas to Methanol. *ACS Sustain. Chem. Eng.* **2014**, *2*, 30–37. [CrossRef]
36. Drouven, M.G.; Grossmann, I.E. Multi-Period Planning, Design, and Strategic Models for Long-Term, Quality-Sensitive Shale Gas Development. *AIChE J.* **2016**, *62*, 2296–2323. [CrossRef]
37. Hao, F.; Zou, H. Cause of Shale Gas Geochemical Anomalies and Mechanisms for Gas Enrichment and Depletion in High-Maturity Shales. *Mar. Pet. Geol.* **2013**, *44*, 1–12. [CrossRef]
38. Li, X.; Pei, C.; Gong, J. Shale Gas Revolution: Catalytic Conversion of C1–C3 Light Alkanes to Value-Added Chemicals. *Chem.* **2021**, *7*, 1755–1801. [CrossRef]
39. Zhang, S.; Wilkinson, L.; Ogunde, L.; Todd, R.; Steves, C.; Haydel, S. *Alkylation Technology Study FINAL REPORT for South Coast Air Quality Management District (SCAQMD), California, USA*; Norton Engineering Consultants, Inc.: Fairfield, NJ, USA, 2016.
40. Albright, L.F. Alkylation-Industrial. In *Encyclopedia of Catalysis*; Howath, I.T., Ed.; John Wiley & Sons, Inc.: Hoboken, NJ, USA, 2010; pp. 226–281.
41. Okuhara, T.; Nishimura, T.; Watanabe, H.; Na, K.; Misono, M. 4.8 Novel Catalysis of Cesium Salt of Heteropoly Acid and Its Characterization by Solid-State NMR. *Stud. Surf. Sci. Catal.* **1994**, *90*, 419–428. [CrossRef]
42. Essayem, N.; Kieger, S.; Coudurier, G.; Védrine, J.C. Comparison of the Reactivities of $H_3PW_{12}O_{40}$ and $H_4SiW_{12}O_{40}$ and Their K^+, NH_4^+ and Cs^+ Salts in Liquid Phase Isobutane/Butene Alkylation. *Stud. Surf. Sci. Catal.* **1996**, *101*, 591–600. [CrossRef]
43. Guo, C.; Liao, S.; Qian, Z.; Tanabe, K. Alkylation of Isobutane with Butenes over Solid Acid Catalysts. *Appl. Catal. A Gen.* **1994**, *107*, 239–248. [CrossRef]
44. Corma, A.; Juan-Rajadell, M.I.; López-Nieto, J.M.; Martinez, A.; Martínez, C. A Comparative Study of O_{42}^{-}/ZrO_2 and Zeolite Beta as Catalysts for the Isomerization of n-Butane and the Alkylation of Isobutane with 2-Butene. *Appl. Catal. A Gen.* **1994**, *111*, 175–189. [CrossRef]
45. Corma, A.; Martinez, A.; Martinez, C. Isobutane/2-Butene Alkylation on MCM-22 Catalyst. Influence of Zeolite Structure and Acidity on Activity and Selectivity. *Catal. Lett.* **1994**, *28*, 187–201. [CrossRef]
46. Flego, C.; Galasso, L.; Kiricsi, I.; Clerici, M.G. TG-DSC, UV-VIS-IR Studies on Catalysts Deactivated in Alkylation of Isobutane with 1-Butene. *Stud. Surf. Sci. Catal.* **1994**, *88*, 585–590. [CrossRef]
47. Unverricht, S.; Ernst, S.; Weitkamp, J. Iso-Butane/1-Butene Alkylation on Zeolites Beta and MCM-22. *Stud. Surf. Sci. Catal.* **1994**, *84*, 1693–1700. [CrossRef]
48. Stöcker, M.; Mostad, H.; Rørvik, T. Isobutane/2-Butene Alkylation on Faujasite-Type Zeolites (H EMT and H FAU). *Catal. Lett.* **1994**, *28*, 203–209. [CrossRef]
49. Rørvik, T.; Mostad, H.; Ellestad, O.H.; Stöcker, M. Isobutane/2-Butene Alkylation over Faujasite Type Zeolites in a Slurry Reactor. Effect of Operating Conditions and Catalyst Regeneration. *Appl. Catal. A Gen.* **1996**, *137*, 235–253. [CrossRef]
50. Chu, Y.F.; Chester, A.W. Reactions of Isobutane with Butene over Zeolite Catalysts. *Zeolites* **1986**, *6*, 195–200. [CrossRef]
51. Weitkamp, J. Isobutane/Butene Alkylation on Cerium Exchanged X and Y Zeolites. *Stud. Surf. Sci. Catal.* **1980**, *5*, 65–75. [CrossRef]
52. Querini, C.A.; Roa, E. Deactivation of Solid Acid Catalysts during Isobutane Alkylation with C4 Olefins. *Appl. Catal. A Gen.* **1997**, *163*, 199–215. [CrossRef]

53. Peng, P.; Stosic, D.; Aitblal, A.; Vimont, A.; Bazin, P.; Liu, X.-M.; Yan, Z.-F.; Mintova, S.; Travert, A. Unraveling the Diffusion Properties of Zeolite-Based Multicomponent Catalyst by Combined Gravimetric Analysis and IR Spectroscopy (AGIR). *ACS Catal.* **2020**, *10*, 6822–6830. [CrossRef]
54. Tonutti, L.G.; Decolatti, H.P.; Querini, C.A.; Dalla Costa, B.O. Hierarchical H-ZSM-5 Zeolite and Sulfonic SBA-15: The Properties of Acidic H and Behavior in Acetylation and Alkylation Reactions. *Microporous Mesoporous Mater.* **2020**, *305*, 110284. [CrossRef]
55. Karge, H.G. Characterization by IR Spectroscopy. In *Verified Syntheses of Zeolitic Materials*; Robson, H., Lillerud, K.P., Eds.; Elsevier Science: Amsterdam, The Netherlands, 2001; pp. 69–71. [CrossRef]
56. Flego, C.; Kiricsi, I.; Parker, W.O.; Clerici, M.G. Spectroscopic Studies of LaHY-FAU Catalyst Deactivation in the Alkylation of Isobutane with 1-Butene. *Appl. Catal. A Gen.* **1995**, *124*, 107–119. [CrossRef]
57. Nivarthy, G.S.; Seshan, K.; Lercher, J.A. The Influence of Acidity on Zeolite H-BEA Catalyzed Isobutane/n-Butene Alkylation. *Microporous Mesoporous Mater.* **1998**, *22*, 379–388. [CrossRef]
58. Dalla Costa, B.O.; Querini, C.A. Isobutane Alkylation with Solid Catalysts Based on Beta Zeolite. *Appl. Catal. A Gen.* **2010**, *385*, 144–152. [CrossRef]
59. Sazama, P.; Pastvova, J.; Kaucky, D.; Moravkova, J.; Rathousky, J.; Jakubec, I.; Sadovska, G. Does Hierarchical Structure Affect the Shape Selectivity of Zeolites? Example of Transformation of n-Hexane in Hydroisomerization. *J. Catal.* **2018**, *364*, 262–270. [CrossRef]
60. Dalla Costa, B.O.; Querini, C.A. Isobutane Alkylation with Butenes in Gas Phase. *Chem. Eng. J.* **2010**, *162*, 829–835. [CrossRef]